Hindawi
Advances in Materials Science and Engineering
Volume 2017, Article ID 3040254, 7 pages
https://doi.org/10.1155/2017/3040254

Research Article

Lattice Dynamics of $Gd_{1-x}Y_xMn_2O_5$ Investigated by Infrared Spectroscopy

Javed Ahmad, Jawaria Mansoor, Mehr Khalid Rehmani, M. Tufiq Jamil, and Syed Hamad Bukhari

Department of Physics, Bahauddin Zakariya University, Multan 60800, Pakistan

Correspondence should be addressed to Syed Hamad Bukhari; bukhari.hamad@gmail.com

Received 7 February 2017; Revised 16 May 2017; Accepted 24 May 2017; Published 21 June 2017

Academic Editor: Peter Majewski

We present infrared (IR) reflectivity of $Gd_{1-x}Y_xMn_2O_5$ with $x = 0$, 0.2, 0.4, 0.6, 0.8, and 1 in the frequency range 30–1000 cm^{-1}. A total of 18 IR active phonons were observed for $GdMn_2O_5$ ($x = 0$) and three additional phonons have been observed with increasing x, marking a total of 21 phonons in YMn_2O_5 ($x = 1$). A systematic investigation was performed to map out the structural distortion through the lattice vibration and discuss the consequences of frequency shifts in phonon modes. In addition, we have calculated the real part of optical conductivity ($\sigma_1(\omega)$) which reflects the semiconducting nature of $Gd_{1-x}Y_xMn_2O_5$.

1. Introduction

Multiferroic materials are promising for future technology due to the simultaneous existence of electric and magnetic orders [1, 2]. Multiferroic RMn_2O_5 received much attention due to strong coupling between magnetic and ferroelectric orders, puzzling magnetic structure, large ferroelectric polarization, and interesting physics [3–5]. At ambient condition, RMn_2O_5 has an orthorhombic structure with *Pbam* space group for a broad range of R ions as shown in Figure 1 [6, 7]. The MnO_6 octahedra are linked in the form of an infinite chain parallel to *c*-axis. However, the chains of MnO_6 are cross-linked with pyramidal MnO_5 with an edge-sharing. The R atoms form an eightfold coordination to oxygen atoms. From high resolution diffraction method it has been found that lattice parameters of RMn_2O_5 system show no significant effect on field or temperature variation [8]. However, the low temperature (below $T_N \sim 40$–45 K) behavior is quite complex, originating from magnetic interaction between $4f$ and $3d$ magnetic moment of R and Mn^{3+}/Mn^{4+} ions, respectively. Below T_N, RMn_2O_5 shows various phase transitions upon temperature variation [5, 9].

In the family of RMn_2O_5, $GdMn_2O_5$ is a unique multiferroic with largest polarization under strong magnetic field among the known multiferroics [3]. Very recently, we have observed a magnetodielectric effect in the paramagnetic phase of $GdMn_2O_5$ [10] as well as in $DyMn_2O_5$ [11]. This unusual magnetodielectric behavior in $GdMn_2O_5$ is consistent with the softening of Raman active phonons, indicating a distinct magnetic correlation slightly above T_N [12]. Moreover, the softening of infrared active modes has also been observed in $DyMn_2O_5$ above T_N [13]. In case of $GdMn_2O_5$, magnetoelectric effect and spin-lattice coupling are commonly acknowledged in several investigations [4, 10, 12, 14]; little is known about the correlations between structural distortion and lattice dynamics. Infrared spectroscopy demonstrates the local lattice distortion and provides the information about the flexible crystalline lattice. Several investigations on IR reflectivity of RMn_2O_5 (R=Tb [15, 16], Dy [13, 17], Ho [18], and Bi [19]) have been performed. In this regard, we are motivated to conduct a systematic investigation of $Gd_{1-x}Y_xMn_2O_5$ and probe the structural distortion through IR phonons. This system is interesting due to many aspects: (i) large difference in ionic radius of Y ($r_Y = 1.019$ Å) and Gd ($r_{Gd} = 1.05$ Å), (ii) large difference in ionic mass of Y ($m_Y = 89$ amu) and Gd ($m_{Gd} = 157$ amu), and (iii) Gd having strongest magnetic moment ($4f$) and Y being nonmagnetic. It is noteworthy to mention that the intermediate members

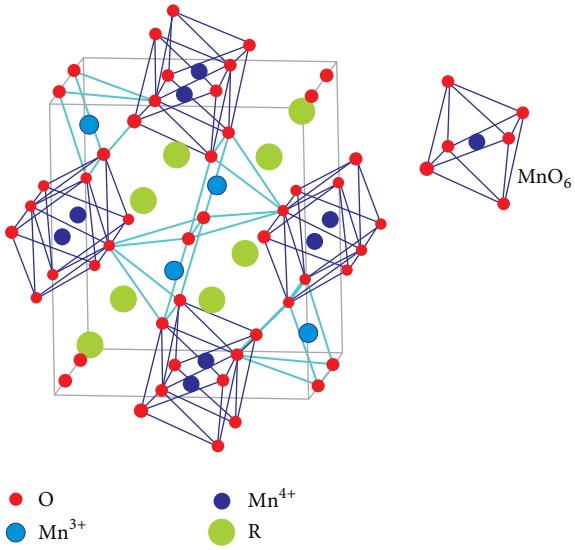

Figure 1: Crystal structure of RMn_2O_5.

($x = 0.2$, 0.4, 0.6, and 0.8) of $Gd_{1-x}Y_xMn_2O_5$ are prepared for the first time, to the best of our knowledge, and are expected to have the same crystal structure as the end members. A detailed investigation of Raman and infrared measurements on $Eu_{1-x}Y_xMnO_3$ system has shown increase in structural distortion from orthorhombic to hexagonal with increasing x ($x > 0.5$) [20]. As majority of vibrational modes are sensitive to structural distortion induced in both Mn polyhedra and with respect to R centers, thus a significant change in the ionic mass and radii at R site would be interesting.

The question whether the continuous substitution of Y into Gd site may lead to any kind of disorder effect due to large difference in mass and ionic radius has not been addressed yet. Therefore, we present lattice dynamics study of $Gd_{1-x}Y_xMn_2O_5$ using the IR reflectivity spectroscopy. The study of optical phonons and their correlation to distortion allows us to have closer look on structural evolution in $Gd_{1-x}Y_xMn_2O_5$.

2. Experiment

$Gd_{1-x}Y_xMn_2O_5$ ceramic samples have been synthesized by using sol-gel method, similar to other RMn_2O_5 compounds [10, 11, 21]. Fourier transform infrared (FTIR) spectrometer (Vertex 80v) has been used to measure the IR reflectivity. Pellets of 13 mm diameter were made smooth prior to spectroscopic measurements. IR reflectivity has been measured in the frequency range of far (30–680 cm^{-1}) and mid (550–7500 cm^{-1}) infrared regions at room temperature under vacuum purge. Detail of measurements can be seen elsewhere [22].

3. Results and Discussion

Figure 2 demonstrates X-ray diffraction (XRD) patterns for the composition $Gd_{1-x}Y_xMn_2O_5$ which exhibit the quite

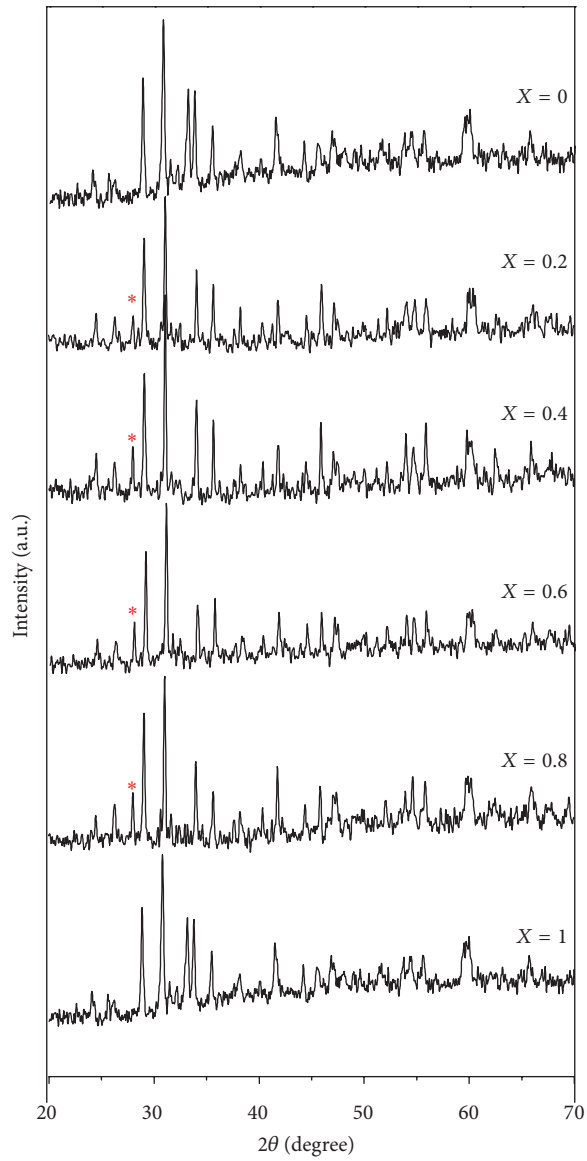

Figure 2: XRD pattern of $Gd_{1-x}Y_xMn_2O_5$ ($x = 0$, 0.2, 0.4, 0.6, 0.8, and 1) at room temperature. ∗ shows the additional peaks not fitted with Rietveld refinement.

similar phase sequences for all concentration x. The obtained XRD patterns have been analyzed by using the Rietveld refinement and the calculated lattice parameters are given in Table 1. A peak at $2\theta \sim 28$ has been identified only for intermediate member of $Gd_{1-x}Y_xMn_2O_5$ ($x = 0.2$, 0.4, 0.6, and 0.8) and is attributed to an additional peak as it was not fitted with the Rietveld refinement (Figure 2). In addition, the peaks at $2\theta \sim 32$ were only found in $x = 0$ and $x = 1$ and well fitted with the Rietveld refinement which remain absent for the intermediate x (Figure 2). However, crystal structure of all members of $Gd_{1-x}Y_xMn_2O_5$ was found to be orthorhombic and the obtained lattice parameters for end members ($GdMn_2O_5$ and YMn_2O_5) of the series $Gd_{1-x}Y_xMn_2O_5$ are in excellent agreement with reported values [23]. As observed, the peak positions slightly shift

Table 1: Summary of lattice parameters and refinement data for $Gd_{1-x}Y_xMn_2O_5$.

X	0	0.2	0.4	0.6	0.8	1
a (Å)	7.35(6)	7.27(6)	7.28(2)	7.29(5)	7.33(5)	7.25(2)
b (Å)	8.54(6)	8.46(3)	8.48(6)	8.48(4)	8.21(2)	8.44(2)
c (Å)	5.69(2)	5.66(4)	5.66(3)	5.64(3)	5.62(5)	5.65(4)
V (Å^3)	357.1	348.2	349.5	348.7	340.2	345.8
R_P	6.57	11.05	11.10	10.62	11.63	6.85
R_{WP}	8.23	13.92	14.03	13.48	14.78	8.62
GOF	1.04	1.06	1.07	1.08	1.11	1.03

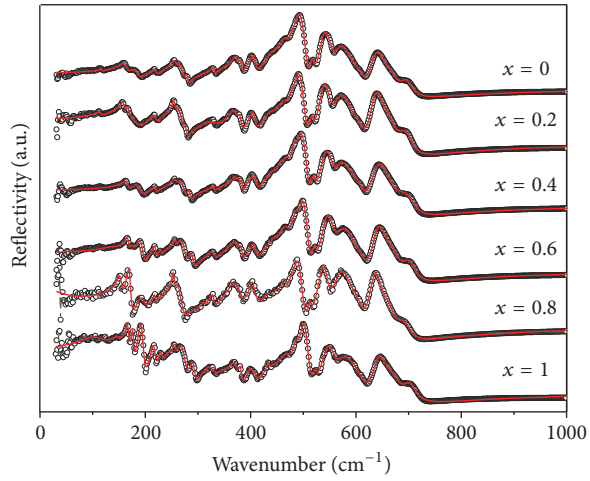

Figure 3: Infrared reflectivity of $Gd_{1-x}Y_xMn_2O_5$ (x = 0, 0.2, 0.4, 0.6, 0.8, and 1) at room temperature. The black open circle shows the experimental curve and the red line shows the fitted data. The spectra are vertically shifted for clarity.

towards low 2θ values with increasing x. Moreover, lattice parameters show a nonmonotonic dependence on x which may be caused by the substitution of small ionic radius of Y into Gd ions which leads to affecting the bond length and bond angle of Mn-O-Mn [9]. These facts are manifesting a structural distortion, which will be of particular focus through IR spectroscopic analysis.

Figure 3 demonstrates the IR reflectivity spectra obtained for $Gd_{1-x}Y_xMn_2O_5$ at room temperature. The experimental spectra were fitted by using Lorentz oscillator model that correlates the optical reflectivity (R) with the dielectric function by Fresnel's formula as

$$R(\omega) = \left| \frac{\sqrt{\epsilon(\omega)} - 1}{\sqrt{\epsilon(\omega)} + 1} \right|^2. \quad (1)$$

To quantify the infrared phonon contribution, the dielectric function $\epsilon(\omega)$ is defined as

$$\epsilon(\omega) = \epsilon_\infty + \sum_j \frac{\omega_{\mathrm{TO},j}^2 S_j}{\omega_{\mathrm{TO},j}^2 - \omega^2 - i\omega\gamma_j}, \quad (2)$$

where ϵ_∞ is the high frequency dielectric constant indicating the contribution to the electronic polarization. $\omega_{\mathrm{TO}(j)}$, S_j, and γ_j are the optical phonon frequency, oscillator strength, and damping factor of jth phonon, respectively. Both (1) and (2) together can give the measured reflectivity spectra. The dispersion parameters ($\omega_{\mathrm{TO}(j)}$, S_j, and γ_j) obtained from the best fit to the experimental curve of $Gd_{1-x}Y_xMn_2O_5$ are summarized in Tables 2 and 3. According to lattice dynamic calculations there are 36 IR active modes in RMn_2O_5 system; however we were able to observe maximum 21 phonons in YMn_2O_5. The origin of this discrepancy simply lies in the polycrystalline nature of our samples having mixed response of all crystallographic axes.

In order to elucidate the lattice dynamics of individual phonon, we have analyzed the ionic displacement within the crystal. Vibrational properties are better understood in the limits of harmonic oscillator $\omega = (k/\mu)^{1/2}$, where k denotes force constant and μ is the reduced mass of the ions involved in the corresponding phonon mode. Thus it is natural to expect that low frequency phonons (≤200 cm^{-1}) are attributed to the vibrations of Gd(Y) and Mn ions, while the intermediate phonon modes are due to the bending and twisting motion of Mn-O polyhedra. At higher frequencies (≥450 cm^{-1}), stretching of the MnO_6 octahedra (including the bending motion of equatorial planes) will contribute to the vibration of phonons [13]. Thus it is expected that substitution of Y into Gd sites always leads to increase in frequency of phonon modes at low frequency due to decrease in reduced mass.

Figure 4 shows a closer look of the low frequency phonon modes dynamics as indicated by arrows. Interestingly, there is a significant increase in frequency for the two most prominent phonon modes ω_{TO1} and ω_{TO3}. Moreover, the mode ω_{TO2} was only observed for $GdMn_2O_5$ at 167 cm^{-1} and almost disappeared and reappeared for YMn_2O_5 at 176 cm^{-1}. Although it shows an increase in the frequency as expected the absence of ω_{TO2} for the intermediate x is quite surprising. One possible explanation is some structural changes that totally damped these mode and is quite reasonable as we have observed some new peaks in XRD patterns at $2\theta \sim 28$ that is only present for intermediate x and thus may be responsible for the absence of ω_{TO2}. The substitution of Y at Gd site takes the system in combined effect of Y/Gd ions that may vibrate in opposite direction relative to Mn polyhedra results in damping the vibration as observed. Moreover, small ionic radius of Y directly affects the Mn-Mn interaction which leads to affecting the relative motion of Y/Gd ions with respect to Mn polyhedral. Thus, a consistent change in both

Table 2: Phonon-fit values of transverse optical mode ω_{TO} (given in cm^{-1}) of the IR reflectivity spectra of $Gd_{1-x}Y_xMn_2O_5$ with x = 0, 0.2, 0.4, 0.6, 0.8, and 1 at room temperature.

ω_{TO}	X						Assignment
	0	0.2	0.4	0.6	0.8	1	
ω_{TO1}	151	165	163	156	161	166	Relative motion of Mn polyhedra and Gd(Y) ions
ω_{TO2}	167	—	—	—	—	176	
ω_{TO3}	194	190	185	166	181	191	
ω_{TO4}	217	217	217	216	218	215	
$\omega_{TO4'}$	—	228	—	—	—	229	
ω_{TO5}	251	255	256	252	255	255	Mn-O bending motions in MnO_6 octahedra
ω_{TO6}	260	267	266	261	265	267	
ω_{TO7}	291	286	282	274	278	289	
ω_{TO8}	327	328	329	325	329	323	
ω_{TO9}	371	370	368	368	370	370	Mn-O twisting motions in Mn polyhedra
$\omega_{TO9'}$	—	380	381	378	379	380	
ω_{TO10}	402	405	406	404	404	399	
ω_{TO11}	433	445	443	439	444	434	
ω_{TO12}	462	464	466	462	463	468	Mn-O bending motions within equatorial
$\omega_{TO12'}$	—	—	—	—	—	486	
ω_{TO13}	484	494	488	486	485	498	MnO_2 equatorial in MnO_6 octahedra
ω_{TO14}	511	519	516	514	514	522	
ω_{TO15}	534	540	536	535	533	545	
ω_{TO16}	565	569	565	565	563	576	Mn-O stretching motions in MnO_6 octahedra
ω_{TO17}	628	633	630	629	629	639	
ω_{TO18}	684	692	681	685	688	697	
ε_∞	2.76	2.95	3.45	2.87	2.92	1.98	
$\varepsilon_\circ$	5.02	5.31	5.45	4.87	5.37	3.41	

Table 3: Phonon-fit values of oscillator strength (S_j) and damping factor (γ_j) of $Gd_{1-x}Y_xMn_2O_5$ with x = 0, 0.2, 0.4, 0.6, 0.8, and 1 at room temperature.

S_j	X						γ_j	X					
	0	0.2	0.4	0.6	0.8	1		0	0.2	0.4	0.6	0.8	1
S_1	0.20	0.14	0.22	0.06	0.25	0.08	γ_1	9.29	7.60	11.22	5.13	14.52	7.69
S_2	0.28	—	—	—	—	0.05	γ_2	8.51	—	—	—	—	5.05
S_3	0.11	0.25	0.28	0.02	0.21	0.17	γ_3	15.14	11.63	16.44	4.14	18.15	11.22
S_4	0.02	0.06	0.04	0.06	0.13	0.02	γ_4	4.46	5.83	4.98	9.10	8.25	11.42
$S_{4'}$	—	0.03	—	—	—	0.03	$\gamma_{4'}$	—	6.28	—	—	—	8.48
S_5	0.05	0.05	0.11	0.06	0.13	0.02	γ_5	4.73	6.80	10.12	6.07	11.35	7.20
S_6	0.22	0.32	0.27	0.24	0.17	0.17	γ_6	18.26	18.35	14.56	17.75	13.43	23.19
S_7	0.01	0.05	0.05	0.02	0.03	0.04	γ_7	10.77	8.09	6.34	7.39	5.94	11.02
S_8	0.05	0.05	0.02	0.18	0.02	0.12	γ_8	9.73	11.12	4.37	43.19	4.06	34.58
S_9	0.27	0.13	0.04	0.16	0.09	0.02	γ_9	27.28	15.93	5.78	19.15	8.80	15.02
$S_{9'}$	—	0.05	0.03	0.03	0.07	0.01	$\gamma_{9'}$	—	9.02	3.83	7.45	7.49	5.11
S_{10}	0.10	0.09	0.16	0.08	0.14	0.01	γ_{10}	12.72	10.93	11.31	11.74	11.07	7.43
S_{11}	0.12	0.04	0.06	0.08	0.16	0.01	γ_{11}	27.72	11.29	9.01	25.40	21.08	4.16
S_{12}	0.10	0.24	0.28	0.20	0.46	0.10	γ_{12}	18.08	20.01	12.50	26.73	20.86	33.51
$S_{12'}$	—	—	—	—	—	0.03	$\gamma_{12'}$	—	—	—	—	—	12.86
S_{13}	0.20	0.12	0.15	0.22	0.16	0.09	γ_{13}	18.25	11.10	9.55	16.25	11.94	17.59
S_{14}	0.01	0.02	0.06	0.02	0.04	0.01	γ_{14}	7.15	7.97	10.57	7.50	9.61	7.12
S_{15}	0.16	0.23	0.34	0.20	0.25	0.09	γ_{15}	17.31	17.99	18.12	17.51	18.29	27.73
S_{16}	0.23	0.25	0.17	0.24	0.14	0.10	γ_{16}	36.58	44.36	29.60	38.71	31.79	46.84
S_{17}	0.08	0.10	0.13	0.10	0.08	0.04	γ_{17}	23.22	21.17	26.74	21.75	23.69	25.80
S_{18}	0.02	0.02	0.05	0.02	0.02	0.14	γ_{18}	32.57	30.59	51.16	32.10	25.94	28.78

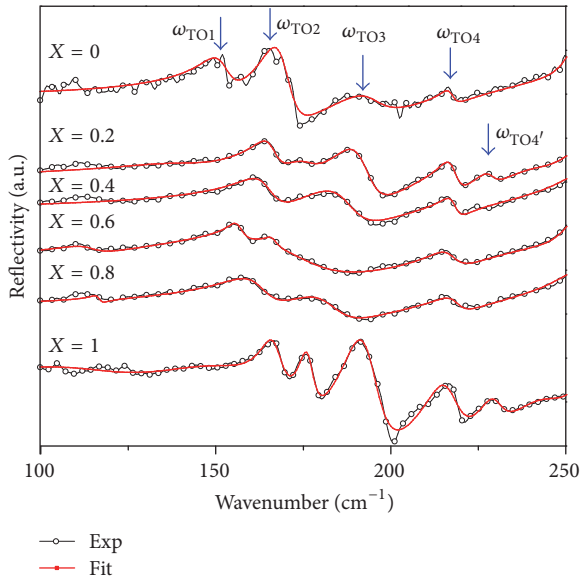

FIGURE 4: Detailed view of the low frequency (<250 cm^{-1}) for $Gd_{1-x}Y_xMn_2O_5$ (x = 0, 0.2, 0.4, 0.6, 0.8, and 1). The black open circle shows the experimental curve and the red line shows the fitted data. Arrows shows the mode evolution with x and the spectra are vertically shifted for clarity.

rare-earth ionic radius and Mn-Mn bond distance may result in damped and discontinuous evolution of frequencies. Thus, we have observed strong lattice dynamics in low frequency range (<200 cm^{-1}) as expected.

With a further insight into lattice dynamics of intermediate frequency modes, one can see that the mode ω_{TO4} shows no obvious frequency shift (Figure 4). Interestingly, a new phonon mode ($\omega_{TO4'}$) has been observed only for x = 0.2 and x = 1 (Figure 4). Moreover, the phonon modes from ω_{TO5} to ω_{TO12} that lies in the intermediate frequency range have shown no significant frequency shift as can be seen from Table 2. More interestingly, corresponding values of S_j and γ_j (j = 5–12) remain almost the same for the complete series $Gd_{1-x}Y_xMn_2O_5$ (Table 3). This simply reflects that Y substitution into Gd sites does not disturb much at higher frequencies. The effect of Y substitution can also be observed in high frequency region as a result of two new phonons. One new phonon ($\omega_{TO9'}$) has been observed for x = 0.2 at a frequency of 380 cm^{-1} and remains almost unchanged with increasing x. The second new phonon is $\omega_{TO12'}$ that has been observed only for YMn_2O_5 at frequency of about 486 cm^{-1}. Thus the origin of three new phonon modes ($\omega_{TO4'}$, $\omega_{TO9'}$, and $\omega_{TO12'}$) after the substitution indicates the strong structural distortion produced, which is difficult to observe in XRD patterns.

In contrast, the high frequency modes ω_{TO13} to ω_{TO18} exhibit strong frequency hardening as shown in Figure 5. These modes represent the stretching and bending motion of MnO_6 octahedra, as in this frequency range, oxygen atoms vibrate as per harmonic oscillator limitation due to its reduced mass as compared to Gd, Y, and Mn ions. While increasing Y content, the whole crystal reduces its volume due to the substitution of lighter element Y into heavy ion Gd. The phonon dynamics is also a function of volume that ultimately gives rise to the change in frequency of phonon modes [24]. Hence, the modes ω_{TO13} to ω_{TO18} harden with decrease in volume, giving rise to stretching of MnO_6 octahedra to vibrate at higher frequency (Figure 5).

We have also calculated the static dielectric constant, which is given by

$$\epsilon_\circ = \epsilon_\infty + \sum_j S_j. \quad (3)$$

$\epsilon_\circ$ represents the static dielectric response obtained from the sum of all the oscillator dielectric strength (S_j) and the electronic polarizability (ϵ_∞). It is important to note that we have observed less number of phonons as compared to those theoretically predicted and thus the dielectric strength of the missing modes must be relatively weaker than those observed. The decrease in $\epsilon_\circ$ with x, similar to the trend of ϵ_∞, is clearly reflecting the small values of the $\sum_j S_j$, which mainly decreases with x (see Figure 6). However, an overall decrease in the value of ϵ_∞ means that energy band gap expands with increasing Y content [24].

We have calculated the real part of optical conductivity (σ_1) through the measured reflectivity spectra by using the relation $\sigma_1(\omega) = \omega\epsilon_2/4\pi$. Here, ω and ϵ_2 are wavenumber and complex part of the dielectric function obtained from measured reflectivity spectra [24]. As a representative, the obtained σ_1 for $GdMn_2O_5$ is shown in Figure 7. It is noteworthy that the spectra have strong absorption peaks, indicating semiconducting behavior of $GdMn_2O_5$. In addition, spectra are structureless below 100 cm^{-1} and have shown no conduction mechanism reflecting the absence of free charge carriers, which is a typical semiconducting nature, in contrast to the Drude-type metallic behavior [25, 26]. Similar behavior has been observed for all samples.

4. Conclusion

We have performed a systematic investigation on structural distortion through lattice dynamics of the phonon modes in $Gd_{1-x}Y_xMn_2O_5$. By utilizing the discriminative sensitivity of IR reflectivity technique, we explicitly observed different types of phonon modes in $Gd_{1-x}Y_xMn_2O_5$ depending upon their symmetry and participating ions. The substitution of Y ion in $GdMn_2O_5$ leads to hardening of phonons caused by the difference in mass and thus decrease in cell volume. Strong movements of Gd(Y) ions exhibit disorder induced effects through low frequency phonons shifts. The Mn sites remain almost unchanged upon increasing x, as reflected through almost constant frequency of the intermediate phonon modes. However, O-ions contribute at higher frequency modes inducing the stretching motion in MnO_6 octahedra caused by change in cell volume. Moreover, optical conductivity indicates the semiconducting nature of the prepared compounds.

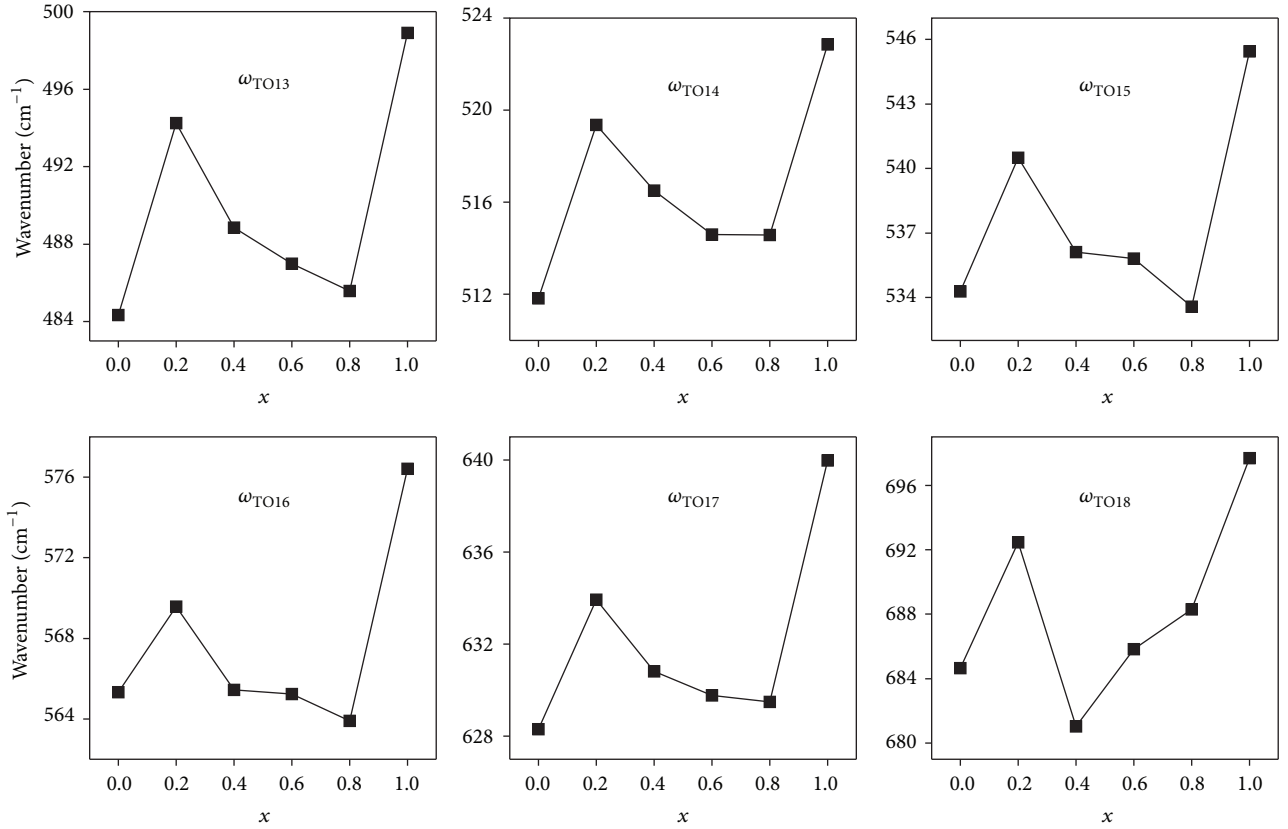

FIGURE 5: Transverse optical frequency (ω_{TO}) of the high frequency phonon mode ω_{TO13} to ω_{TO18} as a function of concentration x.

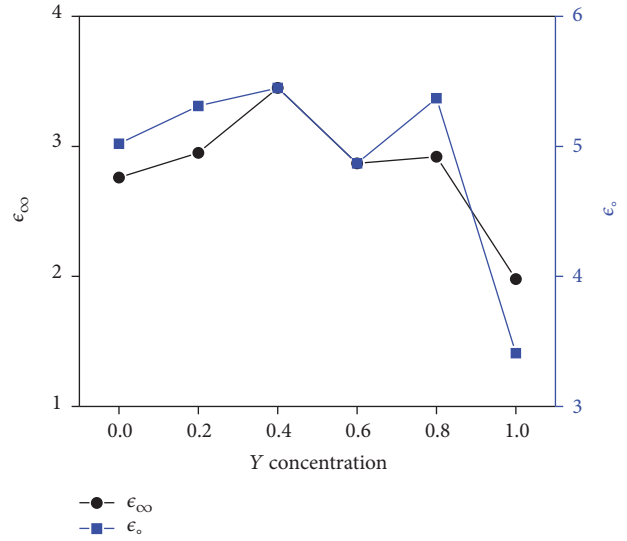

FIGURE 6: The high frequency dielectric constant, ϵ_∞ (closed circle), and static dielectric constant, $\epsilon_\circ$ (closed square), as a function of concentration x.

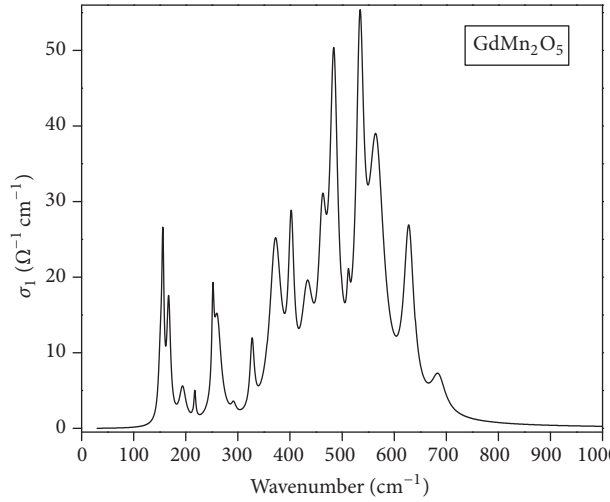

FIGURE 7: Real part of optical conductivity ($\sigma_1(\omega)$) for $GdMn_2O_5$.

Conflicts of Interest

The authors declare that there are no conflicts of interest regarding the publication of this paper.

References

[1] M. Fiebig, "Revival of the magnetoelectric effect," *Journal of Physics D: Applied Physics*, vol. 38, no. 8, pp. R123–R152, 2005.

[2] R. Ramesh and N. A. Spaldin, "Multiferroics: Progress and prospects in thin films," *Nature Materials*, vol. 6, no. 1, pp. 21–29, 2007.

[3] N. Lee, C. Vecchini, Y. J. Choi et al., "Giant tunability of ferroelectric polarization in $GdMn_2O_5$," *Physical Review Letters*, vol. 110, no. 13, pp. 137203–137207, 2013.

[4] S. H. Bukhari, T. Kain, M. Schiebl et al., "Magnetoelectric phase diagrams of multiferroic $GdMn_2O_5$," *Physical Review B - Condensed Matter and Materials Physics*, vol. 94, no. 17, pp. 174446–174453, 2016.

[5] N. Hur, S. Park, P. A. Sharma, S. Guha, and S.-W. Cheong, "Colossal magnetodielectric effects in $DyMn_2O_5$," *Physical Review Letters*, vol. 93, no. 10, pp. 107207–107211, 2004.

[6] A. Munoz, J. A. Alonso, M. T. Casais, M. J. Martínez-Lope, J. L. Martinez, and M. T. Fernandez-Diaz, "Magnetic structure and properties of $BiMn_2O_5$ oxide: a neutron diffraction study," *Physical Review B*, vol. 65, no. 14, pp. 144423–144431, 2002.

[7] J. A. Alonso, M. T. Casais, M. J. Martinez-Lope, J. L. Martínez, and M. T. Fernández-Díaz, "A structural study from neutron diffraction data and magnetic properties of RMn_2O_5 (R = La, rare earth)," *Journal of Physics Condensed Matter*, vol. 9, no. 40, pp. 8515–8526, 1997.

[8] I. Kagomiya, K. Kohn, and T. Uchiyama, "Structure and ferroelectricity of RMn_2O_5," *Ferroelectrics*, vol. 280, no. 1, pp. 131–143, 2002.

[9] M. Tachibana, K. Akiyama, H. Kawaji, and T. Atake, "Lattice effects in multiferroic $R\ Mn_2O_5$ (R = Sm − Dy, Y)," *Physical Review B—Condensed Matter and Materials Physics*, vol. 72, no. 22, pp. 224425–224429, 2005.

[10] S. H. Bukhari and J. Ahmad, "Emergent excitation in the paramagnetic phase of geometrically frustrated $GdMn_2O_5$," *Physica B: Condensed Matter*, vol. 492, pp. 39–44, 2016.

[11] S. H. Bukhari and J. Ahmad, "Evidence for magnetic correlation in the paramagnetic phase of $DyMn_2O_5$," *Physica B: Condensed Matter*, vol. 503, pp. 179–182, 2016.

[12] C. L. Lu, J. Fan, H. M. Liu et al., "An investigation on magnetism, spin–phonon coupling, and ferroelectricity in multiferroic $GdMn_2O_5$," *Applied Physics A: Materials Science & Processing*, vol. 96, no. 4, pp. 991–996, 2009.

[13] J. Cao, L. I. Vergara, J. L. Musfeldt et al., "Magnetoelastic coupling in $DyMn_2O_5$ via infrared spectroscopy," *Physical Review B*, vol. 78, no. 6, pp. 064307–064313, 2008.

[14] N. Poudel, M. Gooch, B. Lorenz, C. W. Chu, J. W. Kim, and S. W. Cheong, "Pressure-induced decoupling of rare-earth moments and Mn spins in multiferroic $GdMn_2O_5$," *Physical Review B - Condensed Matter and Materials Physics*, vol. 92, no. 14, pp. 144430–144436, 2015.

[15] S. Mansouri, S. Jandl, B. Roberge et al., "Micro-Raman and infrared studies of multiferroic $TbMn_2O_5$," *Journal of Physics Condensed Matter*, vol. 28, no. 5, pp. 055901–055907, 2016.

[16] R. Valdés Aguilar, A. B. Sushkov, S. Park, S.-W. Cheong, and H. D. Drew, "Infrared phonon signatures of multiferroicity in $TbMn_2O_5$," *Physical Review B*, vol. 74, no. 18, pp. 184404–184409, 2006.

[17] J. Cao, L. I. Vergara, J. L. Musfeldt et al., "Spin-lattice interactions mediated by magnetic field," *Physical Review Letters*, vol. 100, no. 17, pp. 177205–177209, 2008.

[18] A. A. Sirenko, S. M. O'Malley, K. H. Ahn, S. Park, G. L. Carr, and S.-W. Cheong, "Infrared-active excitations related to Ho^{3+} ligand-field splitting at the commensurate-incommensurate magnetic phase transition in $HoMn_2O_5$," *Physical Review B - Condensed Matter and Materials Physics*, vol. 78, no. 17, pp. 174405–174413, 2008.

[19] F. M. Silva Júnior, C. W. A. Paschoal, R. M. Almeida et al., "Room-temperature vibrational properties of the $BiMn_2O_5$ mullite," *Vibrational Spectroscopy*, vol. 66, pp. 43–49, 2013.

[20] J. A. Moreira, A. Almeida, W. S. Ferreira et al., "Coupling between phonons and magnetic excitations in orthorhombic $Eu_{1-x}Y_xMnO_3$," *Physical Review B - Condensed Matter and Materials Physics*, vol. 81, no. 5, pp. 054447–054459, 2010.

[21] S. H. Bukhari and J. Ahmad, "Magnetoelectric effect in multiferroic $NdMn_2O_5$," *Chinese Physics B*, vol. 26, no. 1, pp. 018103–018106, 2017.

[22] S. H. Bukhari and J. Ahmad, "Infrared active phonons and optical band gap in multiferroic $GdMnO_3$ studied by infrared and UV-visible spectroscopy," *Acta Physica Polonica A*, vol. 129, no. 1, pp. 43–48, 2016.

[23] H. Satoh, S. Suzuki, K. Yamamoto, and N. Kamegashira, "Phase stabilities of $LnMn_2O_5$ (Ln = rare earth)," *Journal of Alloys and Compounds*, vol. 234, no. 1, pp. 1–5, 1996.

[24] J. Ahmad, H. Yamanaka, and H. Uwe, "Bismuth charge disproportionation in semiconducting $BaPb_xBi_{1-x}O_3$ studied by infrared reflection spectroscopy," *Journal of Physics Condensed Matter*, vol. 19, no. 26, Article ID 266223, 2007.

[25] I. Terasaki, T. Nakahashi, A. Maeda, and K. Uchinokura, "Optical study of the doping effect in the metallic oxide $(Nd,Sr)CoO_3$," *Physical Review B*, vol. 43, no. 1, pp. 551–554, 1991.

[26] T. Arima, Y. Tokura, and J. B. Torrance, "Variation of optical gaps in perovskite-type 3d transition-metal oxides," *Physical Review B*, vol. 48, no. 23, pp. 17006–17010, 1993.